

Raman scattering from colliding molecules and Van der Waals dimers in gaseous methane*

A. T. Prengel[†] and W. S. Gornall

Department of Physics, Brandeis University, Waltham, Massachusetts 02154

(Received 14 July 1975)

Raman spectra of low-pressure methane gas both at room temperature and near condensation have been studied in the frequency range from 0 to 50 cm^{-1} . The spectra include two contributions: One is due to collision-induced scattering (CIS) and the other to an unresolved dimer rotational band. The latter component is most prominent at low temperatures. Both the dimer band and CIS spectrum have been computed for a Lennard-Jones interaction and point-dipole polarizability. At large frequency shifts ($> 20 \text{ cm}^{-1}$) it is sufficient to use classical collision dynamics to compute the CIS spectrum, but at lower shifts it is necessary to use quantum theory and add the dimer contribution to obtain good agreement with the experimental spectrum. From analysis of the spectra we determine that the fractional depolarized scattering from dimers is 10% at 300°K and 43% at 115°K. The shape of the far wing (20–50 cm^{-1}) provides a sensitive means of testing the form of the induced polarizability anisotropy. For methane, excellent agreement with experiment is obtained for the point-dipole model.

I. INTRODUCTION

There now exist many articles in the literature that discuss the depolarized intermolecular light scattering from atoms and molecules, known as collision-induced scattering (CIS) or the translational Raman effect. Ever since the early predictions by Levine and Birnbaum¹ that all Raman spectra of gases should have a broad low-frequency component that is due to collision-induced changes in molecular polarizabilities, numerous papers on the subject have appeared dealing with both experimental observations and theoretical interpretations.^{2–9}

It was originally hoped that CIS experiments might provide a sensitive means of testing intermolecular interactions and the form of the collision-induced optical polarizability for atoms and simple molecules. Most theories have concentrated on deriving the spectrum from analytic approximations to the classical dynamics of binary collisions. Unfortunately, in the region of the spectrum where such asymptotic theories are valid, the line shape is exponential and almost model independent.⁸ The only features that can be attributed to either the intermolecular potential or the collision-induced polarizability are slightly different exponents that govern the shape of the spectrum over different frequency ranges. For sufficiently accurate data to detect these small changes in line shape at large frequency shifts it is necessary to perform experiments on high-pressure gas samples (usually greater than 50 atm).

However, it is now quite clear both from theory^{10, 11} and analysis of experiments¹² that at such pressures at least three-body and possibly four-

body interactions play a significant role. Hence, it is even more complicated under these conditions to extract from the CIS spectra of gases at high pressures information about the two-body potential or polarizability.

Most discussions of the collision-induced scattering ignore the possibility of contributions from bound states. Stogryn and Hirschfelder¹³ have determined that for a Lennard-Jones Van der Waals interaction the concentration of dimers in argon, for instance, is approximately 0.1%, at 1 atm and 300 °K. For low concentrations the fraction of dimers is proportional to the density, so that the total average number increases with density squared just as does the total number of collisions per second. Consequently, even at high pressures significant contributions to the Rayleigh wing spectrum from bound states may exist, even though any discrete spectral features attributable to dimers would be observed only at low pressures where pressure broadening is not too severe. Levine¹⁴ has computed the total depolarized scattering from dimers and colliding molecules that interact with a Lennard-Jones potential and finds that for argon at 300 °K this ratio is 10%. The ratio increases significantly if the temperature is lowered.

In this paper we present experimental evidence of the contribution to the Rayleigh wing spectrum of methane (CH_4) arising from the rotational Raman scattering from dimers, and we discuss the relationship between the line shape of the dimer spectrum and the CIS spectrum. First, we show that the classical treatment of the two-body CIS that has been employed by others^{7, 8, 15} in various degrees of approximation provides an excellent

description of the high-frequency wing if precise numerical methods are employed to determine the collision trajectories. Good agreement with spectral data for methane is obtained using the simple point-dipole form for the two-body polarizability. Second, we find that the low-frequency portion of the Rayleigh wing spectrum is made up of two components: a CIS contribution plus a contribution that is due to rotational Raman scattering from Van der Waals dimers. However, to accurately separate these two components, the classical description of the CIS spectrum is inadequate because it does not properly account for low-energy collisions that can quantum-mechanically form metastable bound states. The CIS spectrum is recalculated using quantum theory, and it is found that the low-frequency portion of the CIS spectrum differs from the classically computed spectrum in both intensity and shape. With the improved line shape provided by quantum theory, the CIS spectrum and rotational scattering from dimers can be combined to reproduce the experimental spectra. The fraction of the total depolarized scattering attributed to dimers is thereby determined at high and low temperatures.

The low-pressure experiments with argon by Morgan and Frommhold,¹⁶ similar to those for methane presented here, originally attributed the low-frequency spectrum to scattering from dimers alone. However, more accurate analysis has since shown that at 300 °K their argon spectrum is also dominated by collision-induced scattering.¹⁷

II. EXPERIMENTAL

Experiments have been carried out to study the shape of the Rayleigh wing spectrum of CH_4 at low densities (<10 amagat) and temperatures ranging from 300 °K down to just above condensation. Examples of the spectra are shown in Figs. 1 and 2. Methane was chosen for these experiments because it is a light-spherical-top molecule that has no rotational Raman spectrum and possesses a broad Rayleigh wing spectrum that is easily resolved from the intense Rayleigh line. The low-density spectra of methane presented here are nicely complemented by spectra at higher densities published by Lallemand.⁷

All spectra were excited by a Spectra Physics Model 165 argon-ion laser with an output power of approximately 1 W at 5145 Å. The incident intensity was more than doubled by a simple multi-pass scheme in which the transmitted laser beam is reflected back on itself through the gas cell and off the laser output mirror several times. Light scattered at an angle of 90° into 0.08 sr was passed through a Spex double-grating monochromator and

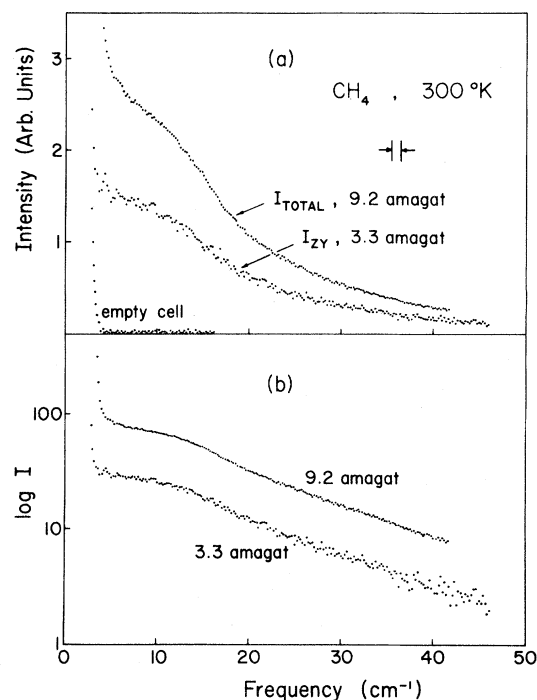


FIG. 1. Stokes Rayleigh wing spectra of CH_4 at 300 °K and densities of 3.3 and 9.2 amagat plotted on (a) linear and (b) logarithmic intensity scales. Dark count has been subtracted. Spectrometer resolution is indicated by the vertical bars.

detected by photon counting using a cooled ITT FW-130 photomultiplier. The photomultiplier dark count was consistently less than 1 per sec. The spectrometer was driven by a digitally controlled stepping motor programmed to step in intervals of approximately 0.2 cm^{-1} . Photon pulses were accumulated on a multichannel scaler which was stepped in conjunction with the spectrometer. A prism polarizer in the laser beam and a polaroid

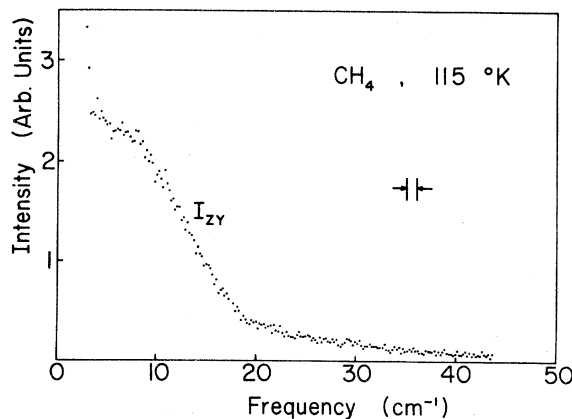


FIG. 2. Stokes Rayleigh wing spectrum of CH_4 at 115 °K and 3.3 amagat with dark count subtracted.

analyzer were used to permit studies in different polarization geometries.

Two gas cells were used. A room-temperature cell was designed for pressures up to 100 atm and was mounted with the laser beam directed vertically through it. The interior of the cell was plated black, and four internal apertures were used to minimize stray light. For low-temperature studies a similar but smaller cell was mounted inside a cryostat filled with pressurized liquid methane. The temperature could be controlled anywhere between 112 and 135 °K to within 0.5° by setting a pressure-relief valve. The laser beam passed through this cell horizontally, so a Dove prism was used to rotate and align the image with the monochromator entrance slit. Methane gas with a minimum purity of 99.9995% was purchased from MG Scientific Gases. The purity was confirmed in our experiments by the total absence of any rotational Raman lines from impurities.

Figure 1 shows the Stokes side of two Rayleigh wing spectra of methane at 300 °K. Although it is not shown here, the spectral intensity scales accurately with density squared at low pressures, as expected for bimolecular processes. The anti-Stokes spectra (not shown) are identical except for a slight intensity asymmetry that is always present because of the Boltzmann factor. All spectra were taken with the incident laser beam propagating in the y direction and polarized in the z direction. Scattering was observed in the x direction. For spectra labeled I_{ZY} , a polaroid analyzer was used to detect only the depolarized (y component) scattering. The higher-density spectrum was taken with no polarizer ($I_{\text{total}} = I_{ZZ} + I_{ZY}$) to maximize the intensity collected. Relative intensities of the two spectra in Fig. 1 are not to scale. Also shown in Fig. 1(a) is the effective Rayleigh line obtained from stray light scattering in the empty cell and scaled to the Rayleigh peak of the 3.3-amagat spectrum. Figure 1(b) shows the two CH_4 spectra plotted logarithmically. Beyond 20 cm^{-1} the line shape is approximately exponential with frequency shift ω and may be represented by $I \sim \exp(-\omega/\omega_0)$, where $\omega_0 = 15.3 \text{ cm}^{-1}$ at either density. It should be noted, however, that the graph of $\log_{10} I$ is actually slightly concave upward beyond 20 cm^{-1} .

It is apparent that these spectra possess line shapes that are distinctly nonexponential below 20 cm^{-1} . At higher densities the methane data of Lallemand⁷ show that this structure persists but becomes less distinct. In the following discussion we show that the structure arises from two effects: scattering from low-energy collisions where the attractive interaction plays a role, and rotational Raman scattering from Van der Waals dimers.

The contribution of the latter is best demonstrated experimentally by studying the spectrum at low temperatures. Figure 2 shows the spectrum of CH_4 at 3.3 amagat and 115 °K (1 °K above condensation). The low-frequency Rayleigh wing is much more intense at this temperature with respect to the wing beyond 20 cm^{-1} . The dramatic change in line shape accompanies an almost fivefold increase in dimer concentration at the lower temperature.¹³ This temperature dependence, together with analysis of spectral line shapes, can be used to distinguish the contributions of dimer rotational Raman scattering from that arising from collision-induced scattering.

III. RAMAN SCATTERING FROM DIMERS

At low densities, to a good approximation, the scattering from dimers and that associated with collisions can be treated separately. This is true because the lifetime of the dimer in a particular quantum state is effectively the time between collisions if we neglect a small fraction of metastable dimers which will dissociate spontaneously in a shorter time.¹³ Consequently, at low densities most dimers live much longer than the duration of a collision, and the dimer Raman spectrum can be derived from the theory of scattering from diatomic molecules. The bimolecular polarizability is defined as¹⁴

$$\alpha_{ij}(\vec{r}_1, \vec{r}_2) = \alpha_{ij}^{(1)}(\vec{r}_1) + \alpha_{ij}^{(2)}(\vec{r}_2) + \alpha_{ij}^{(12)}(\vec{r}), \quad (1)$$

where \vec{r}_1 and \vec{r}_2 are the molecular coordinates and $\vec{r} = \vec{r}_1 - \vec{r}_2$ is the relative coordinate. The first two terms on the right-hand side of Eq. (1) are the polarizabilities of the isolated molecules and are responsible for Rayleigh scattering. Only the third term, the incremental polarizability, produces scattering associated with dimerization. Because of the axial symmetry of the dimer, $\alpha_{ij}^{(12)}(\vec{r})$ has only two independent components, $\alpha_L(r)$ along the symmetry axis and $\alpha_T(r)$ perpendicular to it. For light scattering it is advantageous to decompose $\alpha_{ij}^{(12)}(\vec{r})$ into its spherical average, or isotropic part,

$$\alpha(r) = \frac{1}{3}[\alpha_L(r) + 2\alpha_T(r)], \quad (2)$$

which produces scattering polarized in the same direction as the incident radiation, and its anisotropic part,

$$\beta(r) = \alpha_L(r) - \alpha_T(r), \quad (3)$$

which produces depolarized scattering.

The simplest model of the bimolecular polarizability is the point-dipole model¹⁸ which gives to lowest order

$$\alpha(r) = 4\alpha_0^3 r^{-6}, \quad \beta(r) = 6\alpha_0^2 r^{-3}, \quad (4)$$

where α_0 is the polarizability of a single molecule. It is easy to show that for molecules such as methane $\alpha(r) \ll \beta(r)$ for all realistic values of r . Despite the simplicity of the point-dipole model, this conclusion has been verified experimentally in collision-induced scattering experiments.² Therefore, in computing spectral profiles it is necessary to consider only scattering associated with the anisotropic polarizability $\beta(r)$. Such scattering will be fully depolarized whether it arises from vibrational or rotational transitions between states of the dimer.

Based on these assumptions, the Raman scattering from dimers can be computed from the expression,¹⁹

$$I(v'J'vJ) = AI_0(\omega_0 + \omega)^4 \eta_2 S_J^{J'} N_{vJ} |\langle v'J' | \beta | vJ \rangle|^2. \quad (5)$$

All geometrical and other constant factors, because they are unimportant for the following discussion, are included in the coefficient A . I_0 is the incident intensity at frequency ω_0 , and ω is the Raman frequency shift. The number of dimers per unit volume is given by the factor η_2 which may be computed from a knowledge of the equation of state of the gas.¹³ The final three factors govern the spectral intensity distribution, as they determine the transition probability between the initial and final states designated by the vibrational and rotational quantum numbers vJ and $v'J'$, respectively. The first is a statistical factor having three possible values corresponding to the three allowed rotational transitions,

$$\begin{aligned} S_J^{J+2} &= \frac{3(J+1)(J+2)}{2(2J+1)(2J+3)}, \\ S_J^{J-2} &= \frac{3J(J-1)}{2(2J+1)(2J-1)}, \\ S_J^J &= \frac{J(J+1)}{(2J-1)(2J+3)}. \end{aligned} \quad (6)$$

The last case ($\Delta J = 0$) holds only for $\Delta v \neq 0$. The contribution from trace scattering has been omitted.

The factor N_{vJ} in Eq. (5) is the probability of finding a dimer in the initial state, i.e.,

$$N_{vJ} = (2J+1) e^{-E(v,J)/kT} / Q_{vJ}, \quad (7)$$

where Q_{vJ} is the dimer rotation-vibration partition function. Finally, the term in angular brackets denotes the transition matrix element between the initial and final states:

$$\langle v'J' | \beta | vJ \rangle = \int_0^\infty \psi_{v',J'}^*(r) \beta(r) \psi_{vJ}(r) r^2 dr. \quad (8)$$

In accordance with the above discussion, only the contribution from the anisotropic polarizability $\beta(r)$ is included. The functions $\psi_{vJ}(r)$ and $\psi_{v',J'}(r)$ are the radial intermolecular wave functions associated with the initial and final quantum states of the dimer.

Calculations of the Raman spectrum of methane dimers have been made based on Eqs. (5)–(8). The Lennard-Jones potential with parameters appropriate for methane¹³ ($\sigma = 3.817 \text{ \AA}$ and $\epsilon/k = 148.2 \text{ }^\circ\text{K}$) was chosen to describe the interaction. The effective potential is given by

$$\phi_{\text{eff}} = 4\epsilon [(\sigma/r)^{12} - (\sigma/r)^6] + L^2/2\mu r^2, \quad (9)$$

where $L^2 = J(J+1)\hbar^2$ and μ is the reduced mass of the dimer. Following Stogryn and Hirschfelder,¹³ true bound states have energy $E(v, J) < 0$, whereas dimers bound only by the centrifugal barrier of ϕ_{eff} , that is, with $E(v, J) > 0$, are called metastable because such states can spontaneously dissociate by tunneling. Nevertheless, for all but the few levels near the top of the centrifugal barrier, lifetimes of the metastable states are much greater than 10^{-10} sec ,¹³ typical of the time between collisions at densities of a few amagats. Hence, all metastable levels are included in our computation of the dimer Raman spectrum.

The eigenstates and eigenfunctions for the vibration-rotation states of the methane dimer have been computed by numerical integration of the Schrödinger equation using the Löwdin iteration method.²⁰ The eigenenergies of both stable and

TABLE I. Eigenenergies of the methane Lennard-Jones dimer ($\sigma = 3.817 \text{ \AA}$, $\epsilon/k = 148.2 \text{ }^\circ\text{K}$) in cm^{-1} , accurate to 0.01 cm^{-1} . Positive energies denote metastable levels.

| $J \setminus v$ | 0 | 1 | 2 | 3 | 4 | 5 |
|-----------------|--------|--------|--------|--------|-------|-------|
| 0 | -83.44 | -52.11 | -29.53 | -14.46 | -5.55 | -1.27 |
| 2 | -82.79 | -51.53 | -29.03 | -14.06 | -5.24 | -1.07 |
| 4 | -81.27 | -50.19 | -27.88 | -13.12 | -4.53 | -0.62 |
| 6 | -78.89 | -48.08 | -26.08 | -11.65 | -3.44 | 0.02 |
| 8 | -75.65 | -45.22 | -23.64 | -9.68 | -2.01 | |
| 10 | -71.56 | -41.62 | -20.57 | -7.22 | -0.28 | |
| 12 | -66.62 | -37.28 | -16.91 | -4.33 | 1.61 | |
| 14 | -60.85 | -32.22 | -12.66 | -1.05 | | |
| 16 | -54.26 | -26.48 | -7.88 | 2.51 | | |
| 18 | -46.86 | -20.06 | -2.62 | | | |
| 20 | -38.68 | -13.00 | 3.05 | | | |
| 22 | -29.73 | -5.36 | 8.98 | | | |
| 24 | -20.05 | 2.81 | | | | |
| 26 | -9.67 | 11.43 | | | | |
| 28 | 1.37 | 20.32 | | | | |
| 30 | 13.01 | | | | | |
| 32 | 25.16 | | | | | |
| 34 | 37.68 | | | | | |
| 36 | 50.27 | | | | | |

TABLE II. Matrix elements $|\langle \nu J' | r^{-3} | \nu J \rangle|$ for methane, for Stokes transitions $J' - J = 2$. All wave functions used were normalized to unity.

| $J \backslash \nu$ | 0 | 1 | 2 | 3 | 4 | 5 |
|--------------------|------------------------|------------------------|------------------------|------------------------|------------------------|------------------------|
| 0 | 1.180×10^{-2} | 9.932×10^{-3} | 8.009×10^{-3} | 6.045×10^{-3} | 4.079×10^{-3} | 2.206×10^{-3} |
| 2 | 1.178×10^{-2} | 9.913×10^{-3} | 7.981×10^{-3} | 6.004×10^{-3} | 4.015×10^{-3} | 2.102×10^{-3} |
| 4 | 1.176×10^{-2} | 9.877×10^{-3} | 7.930×10^{-3} | 5.928×10^{-3} | 3.893×10^{-3} | 1.863×10^{-3} |
| 6 | 1.172×10^{-2} | 9.825×10^{-3} | 7.854×10^{-3} | 5.812×10^{-3} | 3.701×10^{-3} | |
| 8 | 1.167×10^{-2} | 9.756×10^{-3} | 7.752×10^{-3} | 5.652×10^{-3} | 3.409×10^{-3} | |
| 10 | 1.161×10^{-2} | 9.667×10^{-3} | 7.619×10^{-3} | 5.434×10^{-3} | 2.901×10^{-3} | |
| 12 | 1.154×10^{-2} | 9.558×10^{-3} | 7.450×10^{-3} | 5.136×10^{-3} | | |
| 14 | 1.145×10^{-2} | 9.426×10^{-3} | 7.237×10^{-3} | 4.700×10^{-3} | | |
| 16 | 1.134×10^{-2} | 9.265×10^{-3} | 6.964×10^{-3} | | | |
| 18 | 1.122×10^{-2} | 9.072×10^{-3} | 6.602×10^{-3} | | | |
| 20 | 1.108×10^{-2} | 8.836×10^{-3} | 6.081×10^{-3} | | | |
| 22 | 1.091×10^{-2} | 8.544×10^{-3} | | | | |
| 24 | 1.072×10^{-2} | 8.164×10^{-3} | | | | |
| 26 | 1.049×10^{-2} | 7.610×10^{-3} | | | | |
| 28 | 1.022×10^{-2} | | | | | |
| 30 | 9.868×10^{-3} | | | | | |
| 32 | 9.374×10^{-3} | | | | | |
| 34 | 8.511×10^{-3} | | | | | |

metastable bound states are listed in Table I. Only every second energy level is tabulated. This is sufficient since the energies are so closely spaced that the fine structure in the spectrum cannot be resolved in the present experiments. For the same reason we neglect effects of nuclear

spin which can cause alternating line intensities or missing alternate lines.

The eigenfunctions or intermolecular wave functions derived from the same calculation have been used to compute the matrix elements $|\langle \nu' J' | \beta | \nu J \rangle|$, based on the point-dipole model [see Eq. (4)]. The results for pure rotational transitions are summarized in Table II. We have also determined that the matrix element for the strongest vibrational transition is approximately five times smaller than that for the strongest pure rotational transition. Including the appropriate Boltzmann factor, this gives a corresponding spectral line intensity ratio of about 30. We therefore conclude, in accord with Frommhold,¹⁷ that the spectral intensity arising from vibrational transitions can be neglected.

Combining the rotational transition matrix elements with the appropriate statistical factors $S_{J'}^{J'}$ and $N_{\nu, J}$ of Eq. (5) yields the spectral profiles shown in Fig. 3. In order to compare these spectra with experimental ones, it is necessary to convolute each component with a broadening function commensurate with the combined instrumental linewidth and lifetime broadening of the dimer states. Doppler broadening is negligible ($< 0.1 \text{ cm}^{-1}$) at temperatures $\leq 300 \text{ }^\circ\text{K}$. Since the dimer lifetimes are not well known but likely produce the dominant broadening, we have chosen to apply a single-Lorentzian broadening function with a full width at half-maximum of Γ . As an example, the resultant dimer Raman spectrum with broadening corresponding to $\Gamma = 4 \text{ cm}^{-1}$ is shown in Fig. 3. Based on the assumptions mentioned

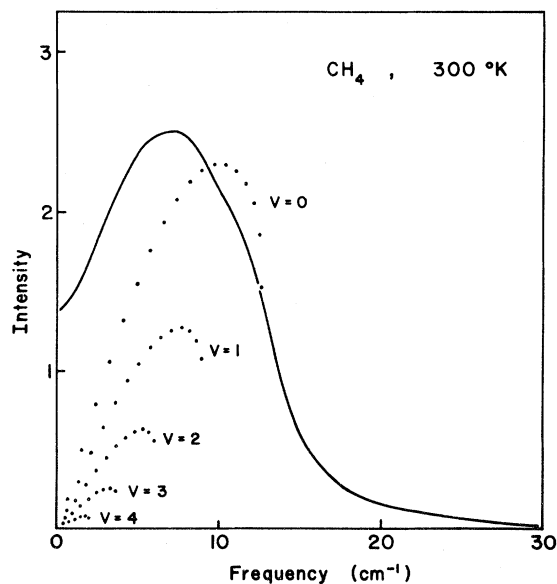


FIG. 3. Theoretical dimer rotational Raman spectrum for CH_4 at $300 \text{ }^\circ\text{K}$. The dots indicate the contribution of particular transitions listed in Table II. The solid curve is the total spectrum after convolution with a Lorentzian profile of width $\Gamma = 4 \text{ cm}^{-1}$, including both Stokes and anti-Stokes contributions.

at the beginning of this section, it should be possible to simply add such a contribution from dimers with the appropriate broadening to the CIS spectrum.

IV. COLLISION-INDUCED SCATTERING

A. Classical theory

Previous attempts^{2,7,8} to explain the observed spectra of CIS in gases have concentrated on using classical collision trajectories to compute the time dependence of $\beta(r)$. The spectral intensity for a particular encounter between two molecules "colliding" with relative velocity v and impact parameter b is given by

$$I(b, v, \omega) = B(\omega_0 + \omega)^4 \left| \int_{-\infty}^{\infty} \beta(r(t)) P_2(\cos \theta(t)) e^{i\omega t} dt \right|^2, \quad (10)$$

where B is a constant, ω_0 is the incident laser frequency, ω is the frequency shift, and $\theta(t)$ is the angular coordinate of the symmetry axis of the pair of molecules in the collision plane measured relative to the orientation at closest approach. $P_2(\cos \theta(t))$ is the second Legendre polynomial. The Fourier transform is evaluated over the entire collision trajectory, taking $t = 0$ to be the time at point of closest approach. Of course, for completeness Eq. (10) should include another term related to the increment in the isotropic polarizability, but for reasons already discussed in Sec. III we continue to neglect it. Finally, the total classical CIS spectrum must be determined by averaging over the Maxwell-Boltzmann velocity distribution and all significant impact parameters, viz.,

$$I(\omega) = \int \int N(b, v) I(b, v, \omega) db dv, \quad (11)$$

where

$$N(b, v) = 2\pi b n^2 (\mu/kT)^{3/2} (2/\pi)^{1/2} v^3 e^{-\mu v^2/2kT}, \quad (12)$$

and n is the number density.

Even with the best analytic approximations for the trajectories⁸ it is impossible to accurately solve these equations using realistic potentials for the low frequency shifts of interest in the present experiments. Consequently, we have numerically integrated the functions $r(t)$ and $\theta(t)$ from Taylor expansions (to the fifth and third derivatives, respectively) to derive accurate trajectories for ϕ_{eff} given in Eq. (9). Classically, the angular momentum $L = \mu vb$. The results of computing $I(\omega)$ for methane at 300 °K using 12 velocities between 0 and 2400 m/sec and 20 impact parameters from 0 to 10 Å are shown in Fig. 4. This is com-

pared with an exponential line shape and the experimental spectrum at 3.3 amagat. There are no free parameters in this computation, and only the absolute intensity has been scaled to match the experimental spectrum at 40 cm⁻¹. Above 20 cm⁻¹ the agreement is excellent, but below that the theoretical spectrum falls below the experimental intensity. However, the maximum difference between the two spectra occurs at too high a frequency to resemble the dimer rotational band discussed in Sec. III.

It should be added that the classical "resonance" phenomenon noted by Frommhold¹⁵ is also prominent in our calculations. Over a range of impact parameters there exists for each case a velocity such that the incident relative energy exactly equals the peak of the centrifugal barrier of the effective intermolecular potential. Classically, such a collision results in an indefinitely orbiting state and a logarithmic singularity in $I(b, v, \omega)$ as the critical combination of b and v is approached. However, it can be shown analytically that combining $I(b, v, \omega)$ with the density of collision states $N(b, v)$ given in Eq. (12) eliminates the singularity, so that computation of the total spectrum is well behaved and the total "resonance" contribution is small. Furthermore, such resonant states imply that the molecules spend an extensive period at a particular separation, which violates the uncertainty principle.

Finally, it should be noted that the classical theory neglects the effect of energy loss or gain owing to emission or absorption of light in the scattering process. Such changes in relative kinetic energy are clearly most significant for low-velocity encounters. Hence, computations involving such collisions must be treated quantum mechanically.

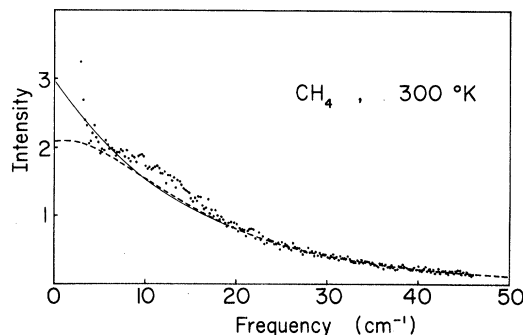


FIG. 4. Comparison of the classical CIS spectrum (---) and exponential line shape (—) with the experimental spectrum (dots) for CH₄ at 300 °K and 3.3 amagat. Both curves are scaled to match the data at 40 cm⁻¹.

B. Quantum theory

The spectral intensity of the collision-induced spectrum may be computed in a manner similar to the bound states with proper modification of

$$I(\omega, E_i, J) = A' \frac{n^2(\omega_0 + \omega)^4}{(\mu T)^{3/2}} e^{-E_i/kT} \left(\frac{3}{2} \frac{(J+1)(J+2)}{2J+3} |\langle E_i + \hbar\omega, J+2 | \beta | E_i, J \rangle|^2 + \frac{3}{2} \frac{J(J-1)}{2J-1} |\langle E_i + \hbar\omega, J-2 | \beta | E_i, J \rangle|^2 + \frac{J(J+1)(2J+1)}{(2J-1)(2J+3)} |\langle E_i + \hbar\omega, J | \beta | E_i, J \rangle|^2 \right), \quad (13)$$

where E_i is the initial relative energy of the colliding pair and A' is a new constant. In deriving Eq. (13) we have introduced the free-particle partition function

$$Q = (V/h^3)(2\pi\mu kT)^{3/2}. \quad (14)$$

As before, the contribution from the isotropic polarizability has been neglected. The total scattering intensity is finally obtained by summing over J and integrating over E_i , viz.,

$$I(\omega) = \int_0^\infty \sum_J I(\omega, E_i, J) dE_i. \quad (15)$$

A computer program has been written that nu-

merically integrates the Schrödinger equation to obtain the wave functions required in Eq. (13) for ϕ_{eff} given in Eq. (9), and calculates the appropriate matrix elements. The integration is carried out using the Numerov method.²¹ Starting at separations of 3 Å (less than the classical turning point), the wave function is computed for increasing distances to the point where the centrifugal contribution to ϕ_{eff} is 99% of the total interaction potential. At this point, the wave function is matched to the corresponding WKB wave function and properly normalized to the free-particle solution at infinity. By utilizing the WKB approximation only for the long-range solution, the error introduced is negligible and a great reduction of

TABLE III. Contributions to the quantum theory CIS Stokes spectrum of methane at 300 °K from different initial relative velocities. Each entry includes the summation over angular momenta. The bottom line is the renormalized total spectrum integrated over initial energies as specified by Eq. (15). Only relative intensities are significant.

| Velocity (m/sec) | Frequency shift (cm ⁻¹) | | | | | | |
|---------------------|---|-------|--------------------|--------------------|--------------------|-------|-------|
| | 0 | 5 | 10 | 15 | 20 | 30 | 40 |
| 50 | 3.792 | 0.489 | 0.208 | 0.109 | 0.068 | 0.031 | 0.016 |
| 100 | 11.170 ^a | 1.844 | 0.702 | 0.381 | 0.232 | 0.104 | 0.053 |
| 200 | 5.850 | 2.710 | 1.011 | 0.524 | 0.314 | 0.138 | 0.070 |
| 300 | 6.690 | 4.961 | 2.299 | 1.156 | 0.663 | 0.276 | 0.133 |
| 400 | 7.093 | 6.198 | 4.195 | 2.263 | 1.233 | 0.464 | 0.211 |
| 500 | 7.849 | 5.522 | 5.955 ^a | 4.250 ^a | 2.247 ^a | 0.679 | 0.280 |
| 600 | 5.619 | 5.479 | 4.383 | 2.992 | 1.814 | 0.687 | 0.308 |
| 700 | 4.767 | 4.553 | 4.043 | 3.136 | 2.127 | 0.873 | 0.381 |
| 800 | 3.775 | 3.658 | 3.370 | 2.701 | 1.973 | 0.899 | 0.406 |
| 900 | 3.020 | 3.003 | 2.799 | 2.366 | 1.868 | 0.927 | 0.421 |
| 1000 | 2.221 | 2.239 | 2.130 | 1.820 | 1.472 | 0.833 | 0.438 |
| 1100 | 1.580 | 1.610 | 1.556 | 1.339 | 1.091 | 0.649 | 0.366 |
| 1200 | 1.116 | 1.129 | 1.470 | 0.985 | 0.820 | 0.520 | 0.301 |
| 1400 | 0.503 | 0.507 | 0.665 | 0.471 | 0.412 | 0.295 | 0.190 |
| 1600 | 0.196 | 0.198 | 0.295 | 0.190 | 0.172 | 0.131 | 0.092 |
| 1800 | 0.068 | 0.068 | 0.104 | 0.067 | 0.063 | 0.050 | 0.038 |
| 2000 | 0.020 | 0.020 | 0.030 | 0.020 | 0.027 | 0.016 | 0.013 |
| $I(\omega)$ | 6.516 | 5.570 | 5.212 | 3.862 | 2.797 | 1.435 | 0.762 |

^a Values that appear slightly anomalous result from particular initial energies nearly resonant with metastable energy levels of the dimer. Such occurrences are few and have only a small influence on the over-all intensity.

computer time is possible.

The results of computations for methane molecules are listed in Table III. Each entry represents the combined matrix elements for $\Delta J = 0, \pm 2$, summed over initial angular-momentum states, i.e., the integrand in Eq. (15). Individual matrix elements were accurate to within $\pm 0.5\%$, but because of the abundance of rotational levels they were not computed for every J . Instead, an appropriate number, dependent on the initial energy, were computed and properly weighted to obtain the entries in Table III. The accuracy was checked by more complete calculations over limited ranges, and results were always consistent to within $\pm 2\%$. The spectral intensity was calculated according to Eq. (15) at seven frequency shifts by integrating over 17 initial relative velocities using Simpson's formula. The integration is sufficiently smooth that the over-all accuracy of the quantum spectrum is estimated to be within $\pm 3\%$. It can be seen from Table III that the low-velocity collisions ($v < 700$ m/sec) produce the dominant contribution to the spectrum at low frequency shifts (< 25 cm^{-1}). Higher-velocity collisions dominate at frequency shifts above 25 cm^{-1} . Therefore, the low-frequency portion of the spectrum is particularly sensitive to the nature of the interaction in the vicinity of the centrifugal barrier and is correctly described only by the quantum theory.

The CIS spectrum for CH_4 obtained from these calculations is shown in Fig. 5. The top diagram shows the separate contributions from transitions for which $\Delta J = 0, \pm 2$ in the spectrum computed at 300°K . The lower diagram compares the quantum-theory line shape with that derived from the

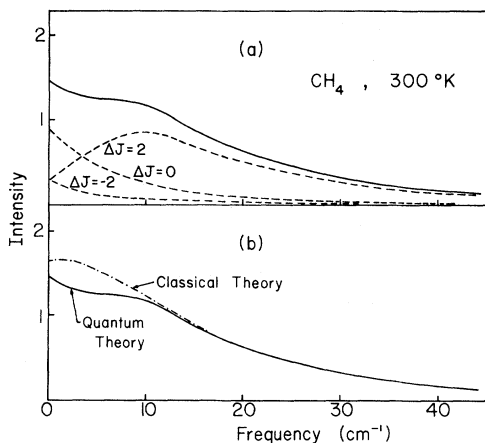


FIG. 5. Quantum theory CIS spectrum for CH_4 at 300°K (a) separated into contributions from $\Delta J = 0, \pm 2$ transitions, and (b) compared with the classical CIS spectrum.

classical theory (Fig. 4). The quantum spectrum is distinctly different from the classical spectrum at low frequency shifts. However, at high frequency shifts (≥ 20 cm^{-1}) the two methods of computation give identical line shapes to within 1% based on the same interaction potential ϕ_{eff} and the same form for the collision-induced polarizability $\beta(r)$.

V. RESULTS AND DISCUSSION

It was not possible to obtain acceptable agreement with the low-frequency Rayleigh wing spectrum of methane using the classical theory of CIS. In Fig. 6 theoretical spectra combining the dimer rotational band and the CIS contribution derived from quantum theory are compared with the observed methane spectra at high and low temperatures. Only the intensity has been adjusted in normalizing these spectra, and this was done independently for the two components. First, the theoretical CIS spectrum was scaled to match the observed intensity at 35 cm^{-1} frequency shift, beyond the range of the dimer rotational band; then the dimer spectrum (convoluted with a Lorentzian broadening function as described in Sec. III) was adjusted to fit the additional intensity observed near 10 cm^{-1} shift and added to obtain the total spectrum. At 115°K , where the dimer component is most prominent, the best fit to the spectrum

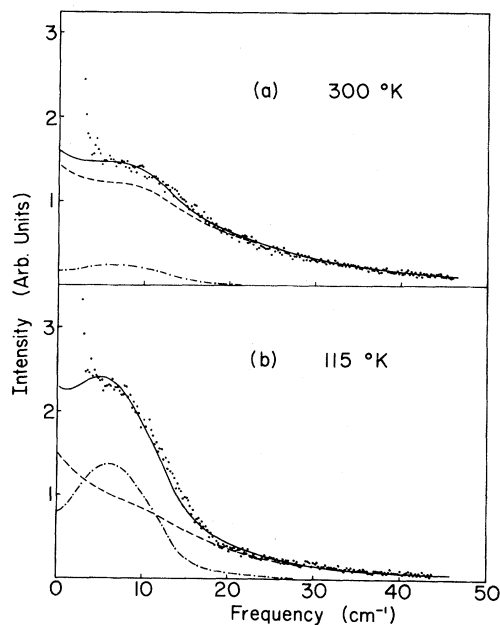


FIG. 6. Comparison of theoretical and observed spectra of CH_4 at 3.3 amagat. The theoretical spectra (—) are separated into contributions from dimers (---) and collisions (-.-).

was obtained for $\Gamma = 4 \text{ cm}^{-1}$. This width is large but it is conceivable that transitions between the closely spaced dimer rotational levels can be induced by very distant collisions ($>10 \text{ \AA}$). At constant density the time between collisions is proportional to $T^{-1/2}$, so a broadening function of $\Gamma = 6 \text{ cm}^{-1}$ was applied in computing the dimer component at $300 \text{ }^\circ\text{K}$.

At both high and low temperatures the agreement with the experimental spectra is good. From this analysis it is possible to determine the fraction of the total integrated intensity that is due to scattering from dimers. At $300 \text{ }^\circ\text{K}$ the fraction is $(10 \pm 2)\%$; at $115 \text{ }^\circ\text{K}$ it is $(43 \pm 3)\%$. These values agree well with Levine's predictions based on spectral moments derived from the division of two-particle phase space.¹⁴ The corresponding values estimated from his curves of the moment $\Gamma_{\beta,0}$ are 13% and 45% .

The agreement between the computed and experimental spectra shown in Fig. 6 is sufficiently good to verify the importance of using quantum theory to derive the low-frequency region of the CIS spectrum. However, beyond 20 cm^{-1} frequency shift in the methane spectrum the classical theory is perfectly adequate, as demonstrated in Fig. 5(b). Furthermore, Lallemand⁷ has shown that the classical spectrum (or equivalently, the time-correlation function) is insensitive to the precise definition of the intermolecular potential for realistic interactions such as the Lennard-Jones or Buckingham models. Our calculations also show that 5% changes in the parameters ϵ and σ in Eq. (9) produce insignificant changes in the CIS line shape. Therefore, in this region of the spectrum where there is no contribution from bound states, it is possible to test the dependence of the spectrum on the form of the collision-induced polarizability based on classical collision dynamics.

The point-dipole model for the induced anisotropic polarizability given in Eq. (4) is accurate provided the interacting pair of molecules is sufficiently far apart. At closer separations higher-order terms may be necessary to account for one or more short-range effects, such as electron overlap, molecular frame distortion, or higher multipole interactions. The relative importance of these effects is not well understood, so for simplicity we add a single term proportional to the next order in the multipole expansion, viz.,

$$\beta(r) = 6\alpha_0^2(r^{-3} + \rho r^{-6}). \quad (16)$$

This form has been used by Gersten^{5,8} and includes only one free parameter ρ to be adjusted to fit the data.

Spectra derived from classical collision dynam-

ics, as outlined in Sec. IV A using Eq. (16) with different values of ρ , are plotted in Fig. 7 and compared with the experimental spectrum for methane at $300 \text{ }^\circ\text{K}$ and 9.2 amagat . All curves have been scaled to match the spectrum at 40 cm^{-1} frequency shift. The slight curvature in the experimental graph of $\log_{10} I$ is reproduced for all three values of ρ but the general slope of the theoretical curves is distinctly sensitive to ρ . This provides an excellent means of testing the form of $\beta(r)$ that has distinct advantages over other techniques. In contrast to measuring the total depolarized scattering intensity, spectral analysis ensures that no error is introduced by depolarized stray light, since light scattered from the cell walls is unshifted in frequency. In addition, only part of the spectrum needs to be analyzed, a part which is unaffected by dimer contributions and yet at low enough frequency shift that good signal-to-noise ratios are possible at moderate gas pressures. This last consideration is important if three-body contributions are to be neglected.

For methane we conclude that $|\rho| < 5 \text{ \AA}^3$. Although no other determinations of the form of $\beta(r)$ for methane are presently available, a comparison can be made with depolarization measurements based on the fact that the integrated depolarized scattering intensity is proportional to²²

$$\langle \beta^2(r) \rangle = \frac{4\pi}{V} \int_0^\infty \beta^2(r) \exp\left(-\frac{U(r)}{kT}\right) r^2 dr. \quad (17)$$

Here V is the scattering volume and $U(r)$ is the

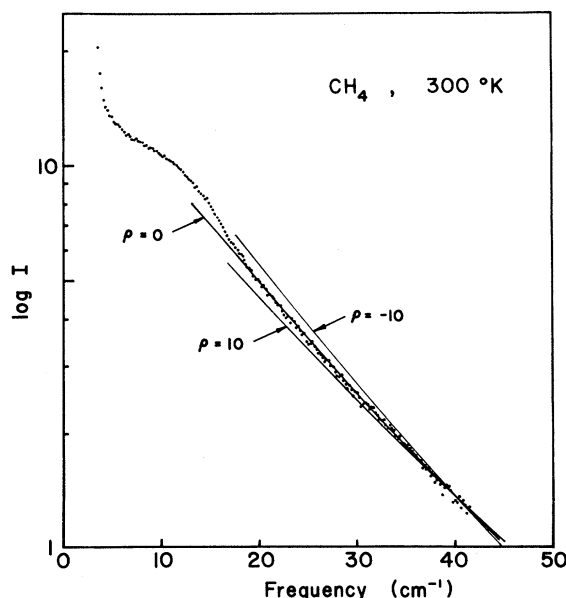


FIG. 7. Shape of the CIS spectrum of CH_4 above 20 cm^{-1} for different models of $\beta(r)$ given by Eq. (16). ρ is in units of \AA^3 .

TABLE IV. Depolarization ratio Δ for CH_4 relative to Δ_0 , calculated using the point-dipole model, for several experimental observations and derived from present CIS line-shape analysis.

| Depolarization ratio | $\Delta_{\text{exp}}/\Delta_0$ | Kerr effect | CIS spectrum | Δ_ρ/Δ_0 | Present results |
|----------------------|--------------------------------|-------------------|-------------------|------------------------|-------------------|
| 1.20 ± 0.17^a | | 0.89 ± 0.07^c | 1.03 ± 0.15^d | | 1.00 ± 0.10^e |
| 0.74 ± 0.03^b | | | | | |

^a Reference 24.

^b Reference 23.

^c Reference 25.

^d Reference 7.

^e Upper and lower bounds obtained from Eq. (17) with $\rho = \pm 5 \text{ \AA}^3$ in Eq. (16).

two-body interaction potential. Thibeau and Oksengorn²³ and recently Watson and Rowell²⁴ have made direct measurements of the total scattering depolarization ratio Δ , and compared it to that derived theoretically for a point-dipole model. Other determinations of Δ have been obtained from the second Kerr virial coefficient by Buckingham and Orr²⁵ and from absolute intensity calibration of the CIS spectrum by Lallemand.⁷ All five results are compared in Table IV. Our result based on $\beta(r)$ falls between the other measurements and has about the same uncertainty.

The coefficient ρ obtained here for methane molecules denotes a much smaller correction to the point-dipole form for $\beta(r)$ than that obtained

from CIS experiments involving rare gases. For instance, Levine and Birnbaum,²⁶ from analysis of CIS spectra of argon based on spectral moments, find that $\beta(r) = 6\alpha_0^2(r^{-3} - 16.5r^{-6.5})$. By comparison, this implies that the form of $\beta(r)$ for methane is much more point-dipole-like than for argon. Experiments on argon of the type presented here are currently in progress to further substantiate this conclusion.

ACKNOWLEDGMENT

We are grateful for helpful discussions with Professors P. Heller, H. N. Pendleton, and L. Frommhold.

*Research supported by the National Science Foundation. The work here is part of a thesis submitted by A. T. Prengel for the Ph.D. degree at Brandeis University in 1975.

[†]Present address: Department of Chemistry, Boston College, Chestnut Hill, Mass. 02167.

¹H. B. Levine and G. Birnbaum, *Phys. Rev. Lett.* **20**, 439 (1968).

²J. P. McTague and G. Birnbaum, *Phys. Rev. Lett.* **21**, 661 (1968); *Phys. Rev. A* **3**, 1376 (1971).

³J. P. McTague, P. A. Fleury, and D. B. Dupré, *Phys. Rev.* **188**, 303 (1969).

⁴P. M. Lallemand, *Phys. Rev. Lett.* **25**, 1079 (1970).

⁵J. I. Gersten, R. E. Slusher, and C. M. Surko, *Phys. Rev. Lett.* **25**, 1739 (1970).

⁶V. Volterra, J. A. Bucaro, and T. A. Litovitz, *Phys. Rev. Lett.* **26**, 55 (1971).

⁷P. M. Lallemand, *J. Phys. (Paris)* **32**, 119 (1971); **33**, C1-257 (1972).

⁸J. I. Gersten, *Phys. Rev. A* **4**, 98 (1971).

⁹D. P. Shelton, M. S. Mathur, and G. C. Tabisz, *Phys. Rev. A* **11**, 834 (1975); D. P. Shelton and G. C. Tabisz, *Phys. Rev. A* **11**, 1571 (1975).

¹⁰W. M. Gelbart, *J. Chem. Phys.* **57**, 699 (1972); *Adv. Chem. Phys.* **26**, 1 (1974).

¹¹C. G. Gray and H. I. Ralph, *Phys. Lett.* **33A**, 165 (1970).

¹²J. P. McTague, W. D. Ellenson, and L. H. Hall, *J.*

Phys. (Paris) **33**, C1-241 (1972).

¹³D. E. Stogryn and J. O. Hirschfelder, *J. Chem. Phys.* **31**, 1531 (1959); **33**, 942 (1960).

¹⁴H. B. Levine, *J. Chem. Phys.* **56**, 2455 (1972).

¹⁵L. Frommhold, *J. Chem. Phys.* **63**, 1687 (1975).

¹⁶C. E. Morgan and L. Frommhold, *Phys. Rev. Lett.* **29**, 1053 (1972).

¹⁷L. Frommhold, *J. Chem. Phys.* **61**, 2996 (1974), and private communication.

¹⁸A. D. Buckingham and J. A. Pople, *Trans. Faraday Soc.* **51**, 1029 (1955).

¹⁹G. Placzek and E. Teller, *Z. Phys.* **81**, 209 (1933); see also G. Herzberg, *Spectra of Diatomic Molecules* (Van Nostrand, Princeton, N. J., 1966), p. 127.

²⁰J. W. Cooley, *Math. Comput.* **15**, 363 (1961); or, for a summary of the method, see J. K. Cashion, *J. Chem. Phys.* **39**, 1872 (1963).

²¹See C.-E. Fröberg, *Introduction to Numerical Analysis* (Addison-Wesley, Cambridge, Mass., 1965), p. 251.

²²See S. Kielich, *Acta Phys. Pol.* **19**, 149 (1960).

²³M. Thibeau and B. Oksengorn, *J. Phys. (Paris)* **33**, C1-247 (1972).

²⁴R. C. Watson and R. L. Rowell, *J. Chem. Phys.* **61**, 2666 (1974).

²⁵A. D. Buckingham and B. J. Orr, *Trans. Faraday Soc.* **65**, 673 (1969).

²⁶H. B. Levine and G. Birnbaum, *J. Chem. Phys.* **55**, 2914 (1971).